

https://doi.org/10.1070/QEL17213

Assessment of the degree of hydration of ocular surface tissues using THz reflectometry

E.A. Kekkonen, A.A. Konovko, E.S. Lee, I.-M. Lee, I.A. Ozheredov, K.H. Park, T.N. Safonova, E.I. Sikach, A.P. Shkurinov

Abstract. **Using the effective medium model, the complex permittivity of the ocular surface system in the THz frequency range is considered. The penetration depth of THz radiation and the sensitivity of the reflected component to the dynamics of evaporation of the tear film are discussed. The results of *in vivo* experiments aimed to determine the reflection coefficient of the ocular surface using continuous THz reflectometers are well described using the developed model.**

Keywords: *ocular surface, THz radiation, effective medium model, cornea of the eye.*

1. Introduction

The term "ocular surface system" was introduced into the medical nomenclature in 2007 based on the work of the International Symposium on Dry Eye Syndrome. The system of the ocular surface is a continuous layer of the epithelium of the cornea and conjunctiva along with the epithelium of the acini of the main and additional lacrimal glands, the epithelium of the lacrimal ducts and meibomian glands. The justification for such a union was the commonality of the embryonic origin of the epithelium of these anatomical structures, the unity of innervation, blood supply, immune and endocrine regulation. The eyelids were also included in the system of the ocular surface, the frequency of blinking movements of which significantly affects not only the formation and spread of the tear film, but also the work of the entire ocular surface [1].

Each of the elements of the ocular surface system takes part in the formation and functioning of the tear film. The tear film, the thickness of which usually does not exceed 10 μm, is not uniform: 98% of its volume is occupied by a liquid, which is the secret of the lacrimal glands and conjunctiva. The outer layer is a thin (0.03–0.50 μm) layer of lipids that protect the tear film from drying out. The inner (water-mucin) layer is water and mucins dissolved in it, which help to keep the tear film on the hydrophobic surface of the corneal epithelium. Even minor changes in any of the elements of the system can cause response changes both in individual substructures and in the entire system of the ocular surface as a whole. This leads to a violation of the composition and properties of the tear film (osmolarity, volume of tear production, acidity, viscosity, surface tension forces, etc.) and causes increased sensitivity, damage to the epithelium of the ocular surface and a tendency to xerosis, i.e., to the development of the 'dry eye' syndrome (DES).

The most common etiological factors of tear film destabilisation include a decrease in the volume of tear production by the lacrimal glands, pathological changes in the corneal epithelium, as well as a violation of congruence between the surfaces of the eyelids and eyes [2]. Violation of the integrity of the ocular surface epithelium contributes to the formation of a large number of inflammatory mediators, leading to the development of an inflammatory process that supports the chronic nature of the damage to the system. DES is a multifactorial disease of the ocular surface, characterised by a decrease in tear film homeostasis and accompanied by symptoms, the development of which is caused by instability of the tear film, hyperosmolarity, inflammation, damage to the ocular surface and sensorineural disorders [3]. Thus, the pathogenesis of DES development is based on the formation of a causal vicious cycle of chronic cytokine-associated inflammation and damage at the cellular level.

The complex pathogenesis and polyetiological nature of DES significantly complicates its diagnosis and the choice of treatment tactics. This emphasises the need to develop reliable diagnostic methods for this disease. This is especially true for methods for studying the tear film, since, as was emphasised above, it plays a key role in maintaining homeostasis of the eye surface. In clinical practice, to assess the stability of the tear film, a test is used to determine its tear break-up time [3]. For a clearer visualisation of the tear film, instillations of a 0.1% sodium fluorescein solution (Norne test) are used. The disadvantages of the method that reduce the accuracy of the data obtained include the irritating effect of the dye on the corneal epithelium, which is an additional factor destabilising the tear film. Later developed alternative non-invasive methods for studying the tear film allow the so-called non-invasive time of rupture to be determined without dropping sodium fluorescein or other drops into the conjunctival cavity, which eliminates the destabilising effect of the dye on the lacrimal film and allows one to obtain the most accurate values of the time of its rupture [1]. Non-invasive research methods include the thioscopy method [4]. Using it, one can not only assess the

E.A. Kekkonen, A.A. Konovko Faculty of Physics and International Laser Center, Lomonosov Moscow State University, Vorob'evy gory, 119991 Moscow, Russia;
Eui Su Lee, Il-Min Lee, Kyung Hyun Park Terahertz Basic Research Section, Electronics and Telecommunications Research Institute (ETRI), Daejeon 305-700, Republic of Korea;
I.A. Ozheredov, A.P. Shkurinov Faculty of Physics and International Laser Center, Lomonosov Moscow State University, Vorob'evy gory, 119991 Moscow, Russia; Institute on Laser and Information Technologies, Russian Academy of Sciences, Division of the Federal Scientific Research Centre 'Crystallography and Photonics', Russian Academy of Sciences, Svyatoozerskaya ul. 1, 140700 Shatura, Moscow region, Russia; e-mail: ozheredov@physics.msu.ru;
T.N. Safonova, E.I. Sikach Research Institute of Ocular Diseases, ul. Rossolimo 11, 119021 Moscow, Russia

Received 27 November 2019
Kvantovaya Elektronika **50** (1) 61–68 (2020)
Translated by V.L. Derbov

stability of the tear film and the thickness of the lipid component, but also determine the quality of the lipid layer. Confocal microscopy, a non-invasive method for studying the cornea, expands the possibilities of studying the corneal anatomy at the level of its microstructure [5]. With the existing advantages of this method, its drawback is the contact of the study and the likelihood of a negative effect of the analgesic on the epithelium of the ocular surface.

In our recent work [6], a diagnostic approach was proposed based on the use of THz radiation obtained by photomixing of radiation frequencies of two continuous narrowband near-infrared lasers. Among other sources of THz radiation, such as a free electron laser, backward wave tube, Gunn diode, THz laser, etc., the photomixer is the most affordable and relatively simple, but at the same time a promising device for generating THz waves [7].

Typically, a THz photomixer [8] consists of two tunable laser sources and a nonlinear element, which provides a signal at the difference frequency in a given THz region. Laser radiation focuses on a nonlinear element, i.e. a semiconductor, in which laser radiation is absorbed and the concentration of free charge carriers increases sharply. In the presence of an applied bias voltage, this leads to the appearance of a current pulse and the generation of THz radiation with a frequency equal to the difference in the radiation frequencies of the used lasers. Solid-state diode lasers with a relatively wide gain band (hundreds of gigahertz and more) are most often used as laser sources [9]. The laser frequency can be adjusted by changing the temperature and/or operating current.

The results of measurements of the reflection coefficient of the cornea of a human eye *in vivo* presented in [6,10] showed a very good sensitivity to the degree of hydration of corneal tissues. It was proposed to use the THz reflectometry method as a diagnostic tool for assessing the dynamics of thinning of the tear film. The penetration depth of THz radiation into the cornea of the eye and the sensitivity of the THz reflectometry method to the thinning of the tear film strongly depend on the frequency of the radiation used [11]. In the present work, within the framework of the proposed method of continuous THz reflectometry, the penetration depth of THz radiation and the sensitivity of the reflected component to the dynamics of evaporation of the tear film are discussed, which is a further development of the proposed non-invasive method for diagnosing the ocular surface.

2. Cornea and tear film

The structure of the ocular surface system is shown in Fig. 1. Histologically, five layers are distinguished in the cornea. The surface layer consists of the anterior stratified epithelium, which is 10%–20% of the thickness of the cornea. The second layer is the Bowman's membrane, i.e. an unstructured, homogeneous, completely transparent, inelastic lamina 6–9 μm thick, sharply delimited from the epithelium. Under the Bowman's membrane is the third layer of the cornea, the stroma, which occupies 90% of its thickness. The fourth layer of the cornea is represented by the posterior limiting lamina, i.e. the Descemet's membrane, which has highly elastic properties and is resistant to damaging factors. The inner membrane of the cornea, the endothelium, acts as a membrane that protects the stroma from penetration of fluid from the anterior chamber.

The cornea of the human eye normally contains 75%–80% water. The remaining 20%–25% falls on collagen with polysaccharides and soluble proteins. Interacting collagen fibrils of the corneal stroma are surrounded by proteoglycan matrices. Non-fibrillar collagen is the main component of the anterior and posterior borders of the corneal membranes. The surface of the cornea is covered with a tear film. This film is most often regarded as another layer of the cornea. A tear film uniformly distributed over the surface of the eye impedes the process of dehydration of the epithelium and disorganization of the collagen structures of the corneal stroma. Changing the degree of hydration of the cornea leads to a violation of its properties, including transparency, which negatively affects visual functions.

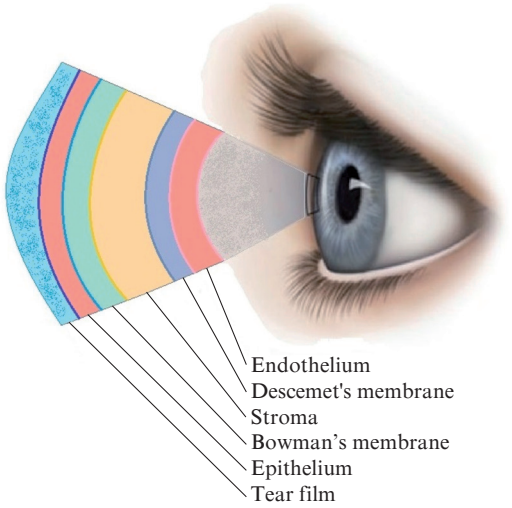

Figure 1. Eye surface system (scale not respected).

3. Model of the effective permittivity

When constructing a model for the interaction of THz radiation and living tissues, it is necessary to take into account its reflection, absorption and scattering. This circumstance significantly complicates the mathematical modelling of the THz response of biological media. In this regard, adequate, but relatively simple models of the permittivity of eye tissues are of considerable interest. For example, the thickness of the cornea of the human eye is significantly less than the wavelength for the frequency range 0.04–0.40 THz. Therefore, in the indicated range, the cornea can be considered a homogeneous medium. This approximation greatly simplifies the modelling of the ocular surface system.

3.1. Relaxation models of the permittivity of bulk water

Water is one of the most important components of the eye. Water permittivity models $\varepsilon(\omega)$ usually include the Debye relaxation terms ($\varepsilon_{\text{relax}}$) and the terms describing the damped oscillators (ε_{osc}) [12].

In the general case, in the THz frequency range, the permittivity of water is given by the expression

$$\varepsilon(\omega) = \varepsilon_\infty + \varepsilon_{\text{relax}} + \varepsilon_{\text{osc}} + \varepsilon_{\text{cond}}, \quad (1)$$

where $\omega = 2\pi f$ is the cyclic frequency of the external electric field; $\varepsilon_\infty = n^2$ is the permittivity in the high-frequency limit;

the term $\varepsilon_{cond} = \sigma/(i\omega\varepsilon_0)$ describes the losses associated with the ionic conductivity σ; and ε_0 is the permittivity of vacuum [13]. Having written Eqn (1) in the form $\varepsilon(\omega) = \varepsilon_{lf} + \varepsilon_{cond}$, we indicate additional restrictions on the amplitudes of the terms in ε_{lf}:

$$\varepsilon_{lf} = \varepsilon_\infty + \sum_m \Delta\varepsilon_m + \sum_i \frac{A_i}{\omega_{0i}^2}, \tag{2}$$

where ε_{lf} is the exactly measured permittivity in the low-frequency limit; $\Delta\varepsilon_m$ is the contribution of the relaxation process with the number m; and A_i/ω_{0i}^2 is the contribution of the damped oscillator with number i, normalised to the oscillator frequency ω_{0i}. It follows from Eqn (2) that the value of ε depends on the number of processes m taken into account and the number of the oscillator i. This is also demonstrated in Fig. 2 presenting the logarithms of the real and imaginary parts of the permittivity of water, as well as the logarithms of the individual components of the permittivity spectrum.

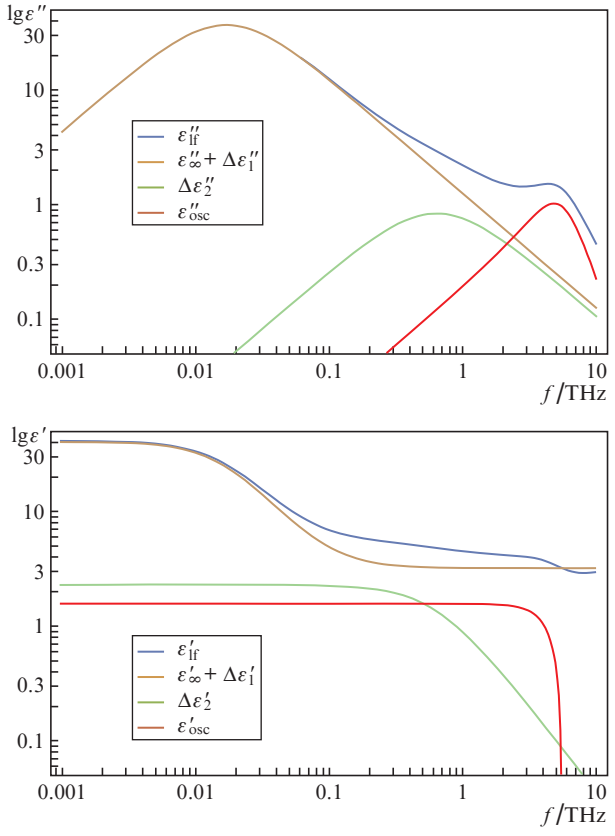

Figure 2. (Colour online) Spectra of the complex permittivity of water.

We can offer the following interpretation of the terms in Eqn (1). The relaxation process described by the term $\varepsilon_{relax} \propto \Delta\varepsilon/(1 + i\omega\tau)$ reflects the collective orientational dynamics of the dipole moment of water molecules, which can be explained as a collective process or a process, in which hydrogen bonds are created and broken. The quantity τ has the meaning of collective orientational relaxation time of hydrogen-bonded bulk water molecules participating in acts of switching hydrogen bonds [14, 15].

The oscillatory process characterised by the term $\varepsilon_{osc} \propto A/(\omega_0^2 - \omega^2 + i\gamma_0\omega)$ describes the vibrational modes of a water molecule with supercritical damping, which correspond to several known vibrational modes in the THz frequency range.

The width of the spectral response of all considered overlapping processes is so great that their centre frequencies (or relaxation times) can only be determined with a large error. In this case, the replacement in the model of the relaxation process by a resonance one allows maintaining an acceptable accuracy of the description of the actual spectrum of the permittivity of water.

3.2. Model of the complex permittivity of the ocular surface system in the THz frequency range based on the effective medium model

Biological objects are usually inhomogeneous, anisotropic, non-periodic, scattering and absorbing in the THz frequency range. However, in a number of important cases, the characteristic sizes of the structural elements of biological media are much smaller than the THz radiation wavelength. This circumstance allows considering such media as homogeneous, and thereby opens up the possibility of simplifying the problem by using the model of 'effective environment'. The simplest models of an effective medium are described by the Maxwell Garnett, Bruggeman, and Landau–Lifshitz–Looyenga equations [16, 17].

The Maxwell Garnett model describes the effective permittivity ε_{eff} of a two-component medium. One component is a homogeneous medium with a permittivity ε_2, the other is a set of spherical particles with a permittivity ε_1. In this case, the Maxwell Garnett equation has the form

$$\frac{\varepsilon_{eff} - \varepsilon_2}{\varepsilon_{eff} + 2\varepsilon_2} = f_1 \frac{\varepsilon_1 - \varepsilon_2}{\varepsilon_1 + 2\varepsilon_2}, \tag{3}$$

where $f_1 = (1/V)\Sigma_i V_i$ is the filling factor; V_i is the volume of the ith particle; and V is the total volume of the composite medium. It is assumed that, firstly, spherical particles do not form clusters and, secondly, they are quite sparse.

The Bruggeman model takes into account the contribution of the permittivity of homogeneous media to the composite in a more symmetrical manner. In addition, this model allows a simple generalisation to the case of a multicomponent medium of spherical particles with different permittivities ε_i. In accordance with the Bruggeman model, the effective permittivity of the medium is determined by the equation

$$\sum_{i=1}^{N} f_i \frac{\varepsilon_i - \varepsilon_{eff}}{\varepsilon_i + 2\varepsilon_{eff}} = 0, \tag{4}$$

where $f_i = (1/V)\Sigma_k V_{ik}$ is the filling factor of the ith fraction and

$$\sum_{i=1}^{N} f_i = 1; \tag{5}$$

V_{ik} is the volume of the kth particle with the permittivity ε_i. It should be noted that the two-component Bruggeman model is valid when the following restrictions on the filling factor are fulfilled:

$$1/3 < f_i < 2/3. \tag{6}$$

The Landau–Lifshitz–Looyenga model for heterogeneous media is described by the equation

$$\varepsilon_{\text{eff}}^{1/3} - \varepsilon_1^{1/3} = f_2(\varepsilon_2^{1/3} - \varepsilon_1^{1/3}), \tag{7}$$

where $\varepsilon_1, \varepsilon_2$ are the permittivities of the bulk materials forming a composite medium.

In addition, one can use the analytical expression proposed by Bergman for porous composites:

$$\varepsilon_{\text{eff}} = \varepsilon_1\left[1 - (1-p)\int_0^1 \frac{g(x,p)\,\mathrm{d}x}{\varepsilon_1/(\varepsilon_1-\varepsilon_2) - x}\right], \tag{8}$$

where p is the porosity; and $g(p,x)$ is the spectral density, which depends on the geometry of the components of the composite medium [18].

The Bruggeman model is more convenient for modelling the dielectric response of multicomponent media. In the case of a medium formed by N components, this model leads to an Nth-order algebraic equation with respect to ε_{eff}s. The choice of root is determined primarily by the sign of the imaginary part of ε_{eff}. For example, Penkov et al. [19] used the Bruggeman model to describe an aqueous solution of proteins:

$$f_{\text{p}}\frac{\varepsilon_{\text{p}} - \varepsilon_{\text{eff}}}{\varepsilon_{\text{p}} + 2\varepsilon_{\text{eff}}} + (1-f_{\text{p}})\frac{\varepsilon_{\text{w}} - \varepsilon_{\text{eff}}}{\varepsilon_{\text{w}} + 2\varepsilon_{\text{eff}}} = 0, \tag{9}$$

where f_{p} and ε_{p} are the filling factor and permittivity of the protein, respectively; ε_{eff} is the permittivity of the aqueous solution; and ε_{w} is the permittivity of the aqueous phase of the solution in the presence of protein. In the simplest case of a two-component medium, equation (4) has two roots:

$$\varepsilon_{\text{eff1,eff2}} = (1/4)[f_1(2\varepsilon_1 - \varepsilon_2) - f_2(\varepsilon_1 - 2\varepsilon_2)] \pm (1/4)\sqrt{8\varepsilon_1\varepsilon_2 + [f_1(\varepsilon_2 - \varepsilon_1) + f_2(\varepsilon_1 - 2\varepsilon_2)]^2}\,. \tag{10}$$

As known, the relaxation times of vibrations of water molecules involved in the hydration of biomolecules differ from the corresponding values for molecules of 'free' (not bound to biomolecules) bulk water [20, 21]. This difference is especially pronounced in the low-frequency region of the absorption and refraction spectra of aqueous solutions [20, 22, 23]. This means that, from the point of view of THz photonics, biological media consist of at least three components: free water, biomolecules and water 'bound' to biomolecules. Each fraction is characterised by a specific permittivity (ε_{bm} for biomolecules, ε_{w} for free water and ε_{bw} for bound water). We can also mention the water of the 'intermediate layer', which differs from the free and bound water by the intermediate value of the relaxation time; however, in certain situations it is possible to neglect some of these components and thereby greatly simplify the calculations. For example, in the case of a structured biological tissue such as dry wood, there is practically no bulk free water, so that the permittivity of bound water can be taken as ε_1, and the permittivity of cell walls can be taken as ε_2, neglecting the contribution of bulk free water molecules [24].

However, in practice it is multicomponent biological media that are of significant interest to researchers. For example, the nerve fibre of the retina includes such components as axon membranes, microtubules, neurofilaments and mitochondria [25]. Moreover, such components of living tissues are usually structured in a certain hierarchical manner. Therefore, we can pose the problem of developing a model of permittivity, taking into account the different spatial scales of the components of the medium.

In many important cases, biological media consist of cells whose characteristic size is much smaller than the radiation wavelength of the THz range. It is also possible that all these cells are elongated in a certain direction. In this case, we can consider the permittivity model with one distinguished direction and two spatial scales [24]. The first spatial scale is associated with cell walls having a permittivity ε_{cw}, and with an intracellular medium with a permittivity ε_{ic}, which can be considered as a homogeneous isotropic medium. Suppose that the cells are elongated in the direction of the z axis, and taking into account optical anisotropy, we use the following expressions for anisotropic permittivity:

$$\varepsilon_{\parallel} = f_{\text{cw}}\varepsilon_{\text{cw}} + f_{\text{ic}}\varepsilon_{\text{ic}}, \tag{11}$$

$$\varepsilon_{\perp} = \varepsilon_{\text{air}}\frac{f_{\text{ic}}\varepsilon_{\text{ic}} + (1+f_{\text{cw}})\varepsilon_{\text{cw}}}{f_{\text{ic}}\varepsilon_{\text{cw}} + (1+f_{\text{cw}})\varepsilon_{\text{ic}}}, \tag{12}$$

where f_{ic} and f_{cw} are volume fractions of cell walls and intracellular medium respectively; $\varepsilon_{\parallel}$ and $\varepsilon_{\perp}$ are the permittivities determining the decrease in the strength of the external electric field applied parallel and perpendicular to the long side of the cell.

The second, smaller, spatial scale is due to the optical properties of the components that form both the cell walls and the intracellular environment. At this stage, we can use the approximation of the effective medium described by the equations

$$\sum_{i=1}^{N_1} f_{\text{cw}i}\frac{\varepsilon_{\text{cw}i} - \varepsilon_{\text{cw}}}{\varepsilon_{\text{cw}i} + 2\varepsilon_{\text{cw}}} = 0, \quad \sum_{i=1}^{N_2} f_{\text{ic}i}\frac{\varepsilon_{\text{ic}i} - \varepsilon_{\text{ic}}}{\varepsilon_{\text{ic}i} + 2\varepsilon_{\text{ic}}} = 0, \tag{13}$$

where $f_{\text{cw}i} = V_{\text{cw}i}/V_{\text{cw}}$ and $f_{\text{ic}i} = V_{\text{ic}i}/V_{\text{ic}}$ are the filling factors of the ith component; $V_{\text{cw}i}$, $V_{\text{ic}i}$ and $\varepsilon_{\text{cw}i}$, $\varepsilon_{\text{ic}i}$ are the volumes and permittivities of the ith component, respectively; and V_{cw} and V_{ic} are volumes of cell walls and intracellular medium, respectively.

One can overcome the limitations of the Bruggeman model related to the spherical shape of the components by addressing the approximation of the ellipsoidal particles by Polder and van Santen [26]. This approach is applicable as long as the condition for quasi-static approximation is satisfied [27].

The efficiency of the 'thin layer' and effective medium approximations in the case of a suspension of biological cells was verified numerically in Ref. [28]. It was shown that both approaches can significantly reduce the resource consumption of the computational problem with good agreement between its solutions and the corresponding analytical results. In particular, modelling the suspension of spherical particles (or spherical cells) forming a cubic lattice by the finite element method in the approximation of a thin layer gives a permittivity that is well consistent with the permittivity calculated from the Pauli–Schwan equation with a filling factor of less than 0.25. It was shown that in the THz wavelength range, the thin layer approximation can be used for cells with a characteristic size greater than 0.1 μm, and the use of the effective medium approximation is promising for modelling the optical properties of cells whose cytoplasm contains spherical vesicles and whose optical properties are isotropic [28].

Generally, an analytical solution for permittivity can be obtained in the case of a sufficiently simple object geometry, for example, for spherical particles [29]. In Ref. [29], the derivation of the formula for permittivity is based on the Laplace transform; analytical expressions are obtained for two char-

acteristic decay times. The developed model can be generalised to multilayer spherical particles. It should also be noted that the optical properties of a composite material, which includes particles with a complex structure, in the general case depend on how the substance and, therefore, the field is distributed in these particles [30].

Consider a simplified three-layer model of the ocular surface system formed by a semi-infinite physiological saline, a cornea 500 μm thick and a tear film with a thickness of not more than 20 μm. Suppose that the permittivity of a tear film and physiological saline is equal to the permittivity of an aqueous NaCl solution with a concentration of 0.9% by volume. From here, based on the Maxwell Garnett model, one can obtain expressions for the permittivities of the cornea in parallel ($\varepsilon_{\|}$) and perpendicular ($\varepsilon_{\perp}$) directions with respect to collagen fibres:

$$\varepsilon_{\|} = f_{\mathrm{w}}\varepsilon_{\mathrm{w}} + f_{\mathrm{col}}\varepsilon_{\mathrm{col}}, \tag{14}$$

$$\varepsilon_{\perp} = \varepsilon_{\mathrm{w}}\frac{(1+f_{\mathrm{col}})\varepsilon_{\mathrm{col}} + (1-f_{\mathrm{col}})\varepsilon_{\mathrm{w}}}{(1-f_{\mathrm{col}})\varepsilon_{\mathrm{col}} + (1+f_{\mathrm{col}})\varepsilon_{\mathrm{w}}}, \tag{15}$$

where $\varepsilon_{\mathrm{col}}$ is the permittivity collagen; f_{w} is the filling factor of the water component; and $f_{\mathrm{col}} = 1 - f_{\mathrm{w}}$. Below, we use the collagen dielectric permittivity model presented in [31].

Assuming that collagen fibres are cylindrical in shape, the model can be used twice to account for free and collagen-bound water. At the first stage, the permittivity $\varepsilon_{\mathrm{cw1}}$ of water with collagen is calculated, the filling factor of which f_1 is taken equal to 0.3. At the second stage, the permittivity of the composite medium $\varepsilon_{\mathrm{cw2}}$ is simulated, formed by a medium with $\varepsilon_{\mathrm{cw1}}$ and collagen with a filling factor $f_2 = 0.1$. Taking into account the dependence of the permittivity of water on temperature and salinity [32], we can calculate the reflection coefficient of the ocular surface as a function of time. In this case, it will be taken into account that the thickness of the lacrimal film changes over time.

4. Equipment for the *in vivo* experiment

In vivo experiments were carried out within the framework of the concept proposed by us in Refs [6, 10] for determining the reflection coefficient of the ocular surface using continuous THz range reflectometers. The layout of the experimental setup for assessing the hydration condition of the ocular surface tissues *in vivo* is presented in Fig. 3.

The basis of the design of the model used was a special ophthalmic stand on which the source and receiver of the THz signal, the lens focusing the THz radiation on the eye surface, and the lens collimating the reflected THz radiation were mounted. Such a stand ensured fixation of the subject's head and coordination of the studied surface of the eye and the focal planes of the THz lenses. The reflection coefficient of the ocular surface was determined at several frequencies of the probe radiation in the range 0.04–0.40 THz. For this purpose, tunable homodyne systems for generating/detecting continuous THz radiation based on diode lasers and semiconductor photomixers were used.

The first system was optimised to operate at 0.04 THz. To generate and detect THz radiation, two PPCL300 (Pure Photonics, USA) distributed-feedback diode (DFB) lasers were used. The presence of such feedback [33] ensured the single-mode single-frequency operation of both lasers in the wavelength range 1530–1531 nm with an average power of 22 mW each, while the oscillation line width did not exceed 10 kHz. Tuning the oscillation wavelength of each of the diode lasers was implemented using the built-in microheater. When the radiation from two cw DFB lasers with close frequencies was mixed, the beats occurred in the optical fibre at the detuning frequency, which was chosen equal to 0.04 THz. The photomixers used in this system to convert the beat signal into THz radiation were based on the InGaAs low-temperature semiconductor with bow-type dipole configuration pads deposited on it (BATOP, Germany). The emitted THz signal was directed through a polyethylene lens with a focal length of 30 mm to the ocular surface at an angle to the normal of 15°. The specularly reflected THz signal was collimated by the second polyethylene lens with the same focal length and sent to the photomixer used to record the radiation. The resulting photocurrent was measured using the synchronous amplifier SR 830 (Stanford Research Systems, USA). The dynamic range of this system was 30 dB.

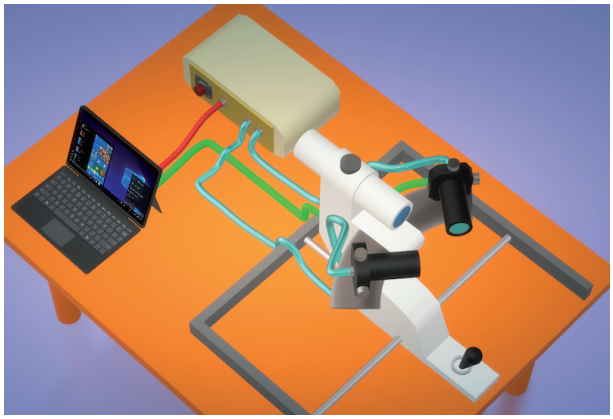

Figure 3. Prototype of the experimental setup for assessing the *in vivo* hydration condition of ocular surface tissues.

The principle of generation and registration of THz radiation in the second system was similar. The main difference was in the design of an optical source produced using dual-mode technology [34] with two phase-matched lasers whose radiation wavelengths were tuned near $\lambda = 1.30$ μm. The log-periodic configuration of photomixers based on the low-temperature InGaAs semiconductor ensured the tuning of the radiation frequency in the range 0.30–0.40 THz while maintaining the dynamic range of ~30 dB. It is necessary to pay attention to the fact that the radiation frequency of the first system (0.04 THz) formally does not correspond to the THz range, but to maintain generality in the future, we will assume that both systems used in the experiment operate in the THz range.

In vivo experiments were conducted in the eyes of subjects who did not have identified eye pathologies and expressed their consent to participate in the studies. During the experiments, the subject's head was fixed. The experimental scenario instructed the subject to keep his eye open as much as possible, and if necessary, he was allowed to blink. For each eye, the reflected THz signal was measured as a function of time. Measurement began at the time of opening the eye and continued for several cycles: 'eye open–eye closed'. The typical observed dynamics of the reflection coefficient of the ocular surface had two clearly visible areas corresponding to the open and closed eye. With an open eye, a decrease was obs-

erved in dependence of the reflection coefficient on time, which corresponds to the dynamics of dehydration. When blinking and in the case of a closed eye, the reflectivity decreases significantly and remains constant until the eye is closed. After opening the eye, reflectivity is restored and becomes the same as in the previous cycle. The obtained dependences of the reflection coefficient on time for the left and right eyes of each subject were averaged over several cycles of 'eye open–eye closed' and recalculated so that in each case the initial moment of time corresponded to the moment of opening the eyes.

5. Results and discussion

Figure 4a shows the results of experimental measurement of the temporal dynamics of a signal reflected from the eye surface at a frequency of 0.04 THz and the result of mathematical modelling of the dependence of the reflection coefficient of the eye on time. It should be noted that the dependence of the reflection coefficient on time is well described by the expression $R = (R_0 - R_\infty)\exp(-t/\tau) + R_\infty$. The difference $R_0 - R_\infty$ characterises the lacrimal film, τ is the time of its thinning, and R_∞ characterises the dry cornea with the remaining eye parameters unchanged during ophthalmological examination.

Using the developed model, we can estimate the penetration depth of THz radiation into the ocular surface system (Fig. 4b). The attenuation depth strongly depends on the frequency and decreases with its growth. Thus, for diagnosing the outer layers of the eye surface (tear film, epithelium, etc.)

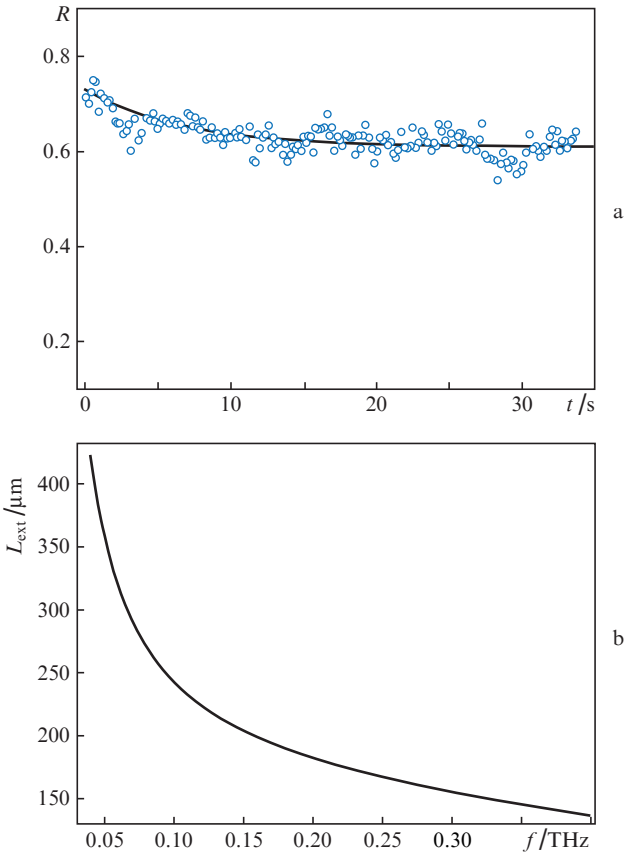

Figure 4. Reflection coefficient of the ocular surface R as a function of time: (points) experimental data and (a) model curve, as well as (b) depth of attenuation of radiation L_{ext} as a function of its frequency.

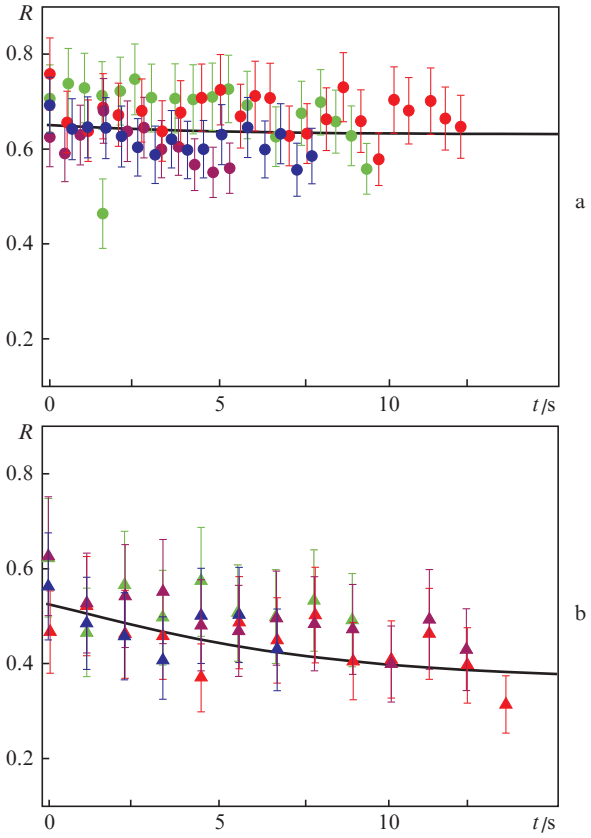

Figure 5. Tested eye reflection coefficients for radiation frequencies (a) 0.04 and (b) 0.40 THz: (points) experimental data and (curves) numerical simulation results.

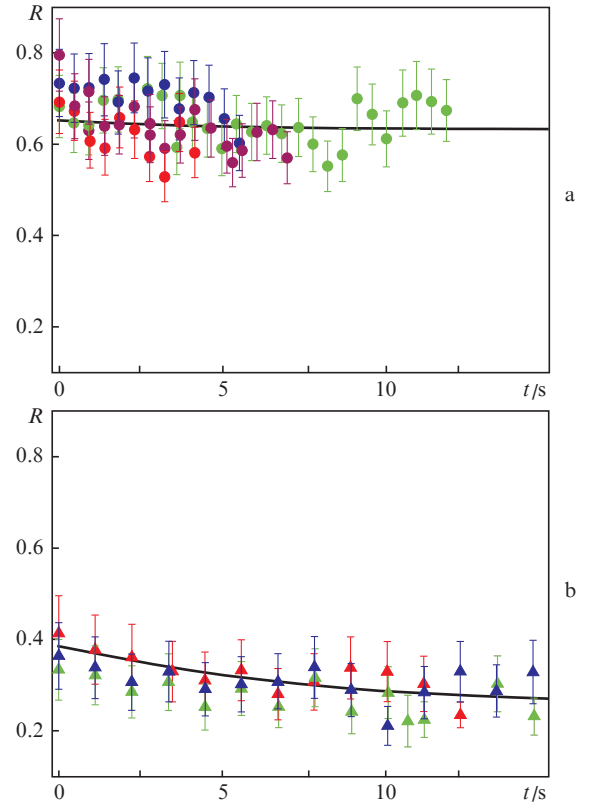

Figure 6. Same as in Fig. 5, but for the subject's other eye.

relatively higher frequencies (0.30–0.40 THz) are often preferable. Note that at the indicated frequencies, the depth of radiation penetration remains less than the thickness of the cornea; however, the contribution of the cornea to the reflected signal undoubtedly remains noticeable.

Although the experimentally obtained series of averaged values of the reflection coefficient from the eyes of different subjects differ significantly, the developed model is in good agreement with the experiment (Figs 5 and 6).

Note that the reflection coefficient depends on time rather weakly. However, the absolute value of the difference between the initial value of the reflection coefficient and reflection coefficient at an arbitrary instant of time, $\Delta R = |R(0) - R(t)|$, has a noticeable value at high frequencies (Fig. 7).

In the linear approximation of the theoretical model, the reflection coefficient at large times is determined by the cornea, and its decrease in the beginning is determined by the characteristics of the water layer. For frequencies 0.04 and 0.40 THz, a monotonic change in the refractive index is observed in the temporal dynamics due to a monotonic change in the thickness of the tear film (with its drying). The quantitative differences in the values of the reflection coefficient are due, in particular, to the frequency dispersion of the refractive indices (water and the cornea) and the different depth of penetration of radiation into the cornea (due to changes in the radiation wavelength and its absorption coefficient). It should be noted that a sharp rupture (disappearance) of the tear film was not studied in this work, since no abrupt change in the refractive index was observed within the measurement errors. The difference in reflection coefficients at (relatively) low and high frequencies is more clearly demonstrated by the rate of reflection coefficients change (Fig. 8). This circumstance serves as an additional argument for the use of radiation with relatively higher frequencies (0.30–0.40 THz) for the diagnostics of the outer layers of the ocular surface. In particular, radiation at a frequency of 0.40 THz is suitable for diagnosing the state of a tear film.

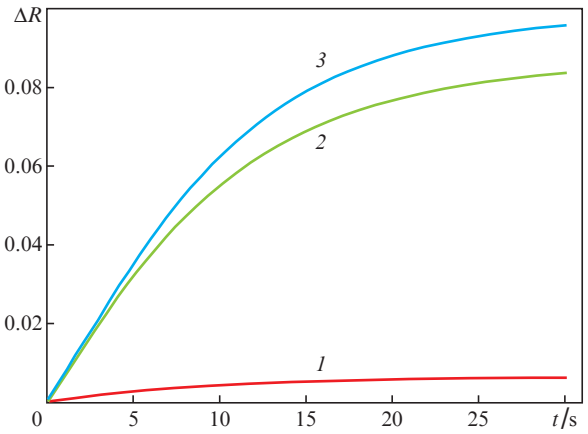

Figure 7. Dependences $\Delta R = |R(0) - R(t)|$ for the radiation at frequencies (*1*) 0.04, (*2*) 0.30 and (*3*) 0.40 THz.

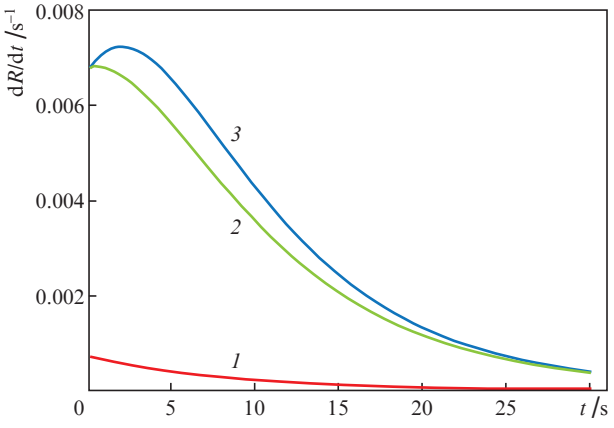

Figure 8. Rates of change of reflection coefficients as a function of time for radiation at frequencies (*1*) 0.04, (*2*) 0.30 and (*3*) 0.40 THz.

6. Conclusions

According to the results of *in vivo* experiments using continuous THz radiation and numerical simulation, the sensitivity of the reflected component of THz radiation at different frequencies to the dynamics of evaporation of the tear film and to the degree of hydration of the ocular surface tissues was demonstrated. This is another important argument in favour of the need for further development of the proposed diagnostic non-invasive method for assessing the condition of the ocular surface.

Acknowledgements. This work was partially supported the Russian Foundation for Basic Research (Project Nos 17-29-02487–, 18-02-00528 and 17-00-00270 KOMFI), the Moscow University Development Programme until 2020, the Basic Research Programme of the Presidium of the Russian Academy of Sciences No. 56 and the Ministry of Science and Higher Education of the Russian Federation in the framework of the State Assignment of the Federal Research Centre for Crystallography and Photonics of the Russian Academy of Sciences.

References

1. Stern M.E., Gao J., Siemasko K.F., Beuerman R.W., Pflugfelder S.C. *Exp. Eye Res.*, **78**, 409 (2004).
2. Brzheskii V.V., Egorova G.B., Egorov E.A. *Sindrom 'sukhogo glaza' i zabolevaniya glaznoi poverkhnosti: klinika, diagnostika, lechenie* (*Dry Eye Syndrome and Ocular Surface Disease: Clinic, Diagnosis, Treatment*) (Moscow: GEOTAR-Media, 2016).
3. Bhavsar A.S., Bhavsar S.G., Jain S.M. *Oman J. Ophthalmology*, **4**, 50 (2011).
4. Craig J.P., Tomlinson A. *Optom. Vis. Sci.*, **74**, 8 (1997).
5. Bohnke M., Masters B.R. *Prog. Retin. Eye Res.*, **18**, 553 (1999).
6. Ozheredov I., Prokopchuk M., Mischenko M., et al. *Laser Phys. Lett.*, **15**, 055601 (2018).
7. Mittleman D. *Sensing with THz Radiation* (Berlin: Springer, 2003).
8. Plinski E.F. *Bull. Pol. Acad. Sci.*, **58**, 463 (2010).
9. Sands D. *Diode Lasers* (London: Taylor & Francis, 2004).
10. Smolyanskaya O.A., Chernomyrdin N.V., Konovko A.A., et al. *Prog. Quantum Electron.*, **62**, 1 (2018).
11. Taylor Z.D., Garritano J., Sung S., et al. *IEEE Trans. Terahertz Sci. Technol.*, **5**, 170 (2015).
12. Raicu V., Feldman Y. *Dielectric Relaxation in Biological Systems: Physical Principles, Methods, and Applications* (Oxford: Oxford University Press, 2015).
13. Penkov N., Shvirst N., Yashin V., et al. *J. Phys. Chem. B*, **119**, 12664 (2015).
14. Shiraga K., Adachi A., Nakamura M., et al. *J. Chem. Phys.*, **146**, 105102 (2017).
15. Leitner D.M., Gruebele M., Havenith M. *HFSP J.*, **2**, 314 (2008).

16. Golovan' L.A., Timoshenko V.Yu., Kashkarov P.K. *Phys. Usp.*, **50**, 595 (2007) [*Usp. Fiz. Nauk*, **177**, 619 (2007)].
17. Markel V.A. *J. Opt. Soc. Am. A*, **33**, 1244 (2016).
18. Bergman D.J. *Annals Phys.*, **138**, 78 (1982).
19. Penkov N., Yashin V., Fesenko E., et al. *Appl. Spectrosc.*, **72**, 257 (2018).
20. Singh R., George D.K., Benedict J.B., et al. *J. Phys. Chem. A.*, **116**, 10359 (2012).
21. Heyden M., Brundermann E., Heugen U., et al. *J. Am. Chem. Soc.*, **130**, 5773 (2008).
22. Born B., Havenith M. *J. Infrared, Millimeter, Terahertz Waves*, **30**, 1245 (2009).
23. Shiraga K., Ogawa Y., Suzuki T., et al. *Appl. Phys. Lett.*, **102**, 053702 (2013).
24. Zolliker P., Ruggeberg M., Valzania L., Hack E. *IEEE Trans. Terahertz Sci. Technol.*, **7**, 722 (2017).
25. Zhou Q., Knighton R.W. *Appl. Opt.*, **36**, 2273 (1997).
26. Polder J., van Santeen J.H. *Physica*, **12**, 257 (1946).
27. Scheller M., Wietzke S., Jansen C., Koch M. *J. Phys. D: Appl. Phys.*, **42**, 065415 (2009).
28. Asami K. *Jpn. J. Appl. Phys.*, **49**, 127001 (2010).
29. Sun T., Gawad S., Green N.G., Morgan H. *J. Phys. D: Appl.Phys.*, **40**, 1 (2007).
30. Apresyan L.A., Vlasov D.V. *Tech. Phys.*, **62**, 6 (2017) [*Zh. Tekh. Fiz.*, **87**, 10 (2017)].
31. Yang K., Chopra N., Abbasi Q.H., et al. *IEEE Access*, **5**, 27850 (2017).
32. Lunkenheimer P., Emmert S., Gulich R., et al. *Phys. Rev. E*, **96**, 062607 (2017).
33. Nanii O.E. *Lightwave Russian Edition*, **2**, 48 (2003).
34. Kim N., Han S.P., Ko H., et al. *Opt. Express*, **19**, 15397 (2011).